UCRL - 75623
PREPRINT

Conf-740809--5

LAWRENCE LIVERMORE LABORATORY
University of California / Livermore, California

X-RAY FLUORESCENCE EXPERIMENTS WITH POLARIZED X RAYS

R. H. Howell
W. L. Pickles
J. L. Cate, Jr.

July 15, 1974

This paper was prepared for submittal to Proceedings of Applications of X-ray Analysis, Denver, CO, Aug. 7-9, 1974.

X-RAY FLUORESCENCE EXPERIMENTS WITH POLARIZED X RAYS*

R. H. Howell, W. L. Pickles, and J. L. Cate, Jr.

Lawrence Livermore Laboratory, Univ. of California

Livermore, California 94550

ABSTRACT

Two methods of obtaining polarized x rays for fluorescence experiments are discussed. Compton scattering from a low-Z scatterer is the usual method used in such experiments. The polarization of x rays undergoing anomalous Borrman transmission in a dislocation-free crystal is also described and preliminary results are presented. Approximate expressions, useful for comparing scatter-polarizing systems, are derived for the dependence of scatter rejection and fluorescent efficiency on two scattering-system parameters: the thickness of the scattering polarizer and the geometric limit to solid angles and angular divergences in the system.

INTRODUCTION

Several experimenters have demonstrated that the ratio of background x rays scattered from a sample to the sample's fluorescent signal may be significantly reduced by polarizing the excitation flux and positioning the detector in an appropriate geometry. (1, 2, 3) The polarizing mechanism used in all such experiments has been Compton scattering, at 90° to the unpolarized beam direction, from a low-Z scatterer.

Certain parameters in the scattering system are important in determining both the scatter rejection (see Table I for definitions) and the fluorescent efficiency. The two most important parameters are the thickness of the scattering polarizer (T_p) and the geometric limit to solid angles and angular divergences in the system (ω, ω', γ).

*Work performed under the auspices of the U.S. Atomic Energy Commission.

Table 1. Definition of terms.

Scattering fraction $\equiv \dfrac{(I_{sc}/I_{fl})\big\vert_{polarized}}{(I_{sc}/I_{fl})\big\vert_{unpolarized}}$	Scattered intensity, normalized to fluorescent signal intensity, for polarized relative to unpolarized excitation.
$R_g \equiv$ contribution to scattering fraction due to geometry: a function of ω, ω', γ.	
$R_s \equiv$ contribution to scattering fraction due to multiple scattering: a function of T_p.	
$\omega, \omega', \gamma \equiv$ one-half the range of the scattering-system angles θ, θ', Γ about 90°.	
$T_p \equiv$ the thickness of the polarizing scatterer.	
Scatter rejection = amount of reduction in the scattering fraction.	
Fluorescent efficiency $\equiv \dfrac{(I_{fl})\big\vert_{polarized}}{(I_{fl})\big\vert_{unpolarized}}$	Fluorescent intensity for polarized relative to unpolarized excitation.

We discuss the relationships of these parameters to scatter rejection and to fluorescent efficiency, and we derive approximate expressions, useful for comparing systems, for these relationships.

Because of limitations in scattering as a practical polarizing mechanism, a second possible source of polarized x rays has been explored: x rays undergoing anomalous Borrman transmission in a dislocation-free crystal are polarized. This effect is described and preliminary results are presented.

Polarization by Scattering

The classical cross section for scattering linearly polarized x rays through an angle θ is

$$d\sigma/d\Omega = r_o^2$$

for polarization normal to the scattering plane and

$$d\sigma/d\Omega = r_o^2 \cos^2 \theta$$

for x rays polarized in the scattering plane, where θ is the scattering angle and r_o is the electron radius. The corresponding cross sections for Compton scattering have an added energy-dependent term which is angle-independent in the in-plane cross

section. This term is small (0.5% at 40 keV and less at lower energies) and its effect will not be considered in the remainder of this paper.

Thus, one scatter through 90° results in a beam polarized normal to the first scattering plane. A detector may then be positioned so that this polarization is in the plane of any subsequent scattering from the sample, resulting in less scattering into the detector. This geometry is shown in Fig. 1.

Solid Angle and Angular Divergence

Scattering into the detectors from the sample is at a minimum when the scattering angles (θ and θ') and the angle between scattering planes (Γ) are all 90°. The collimation of the x-ray source, polarized beam, and detector define limits on the ranges of these angles. By integrating the classical cross section over the range of each angle, an expression may be obtained for the geometric scattering fraction, R_g: the ratio of scattering into the detector (relative to flux incident on the sample) for polarized versus unpolarized excitation. In the limit of small angles the scattering fraction due to geometry* is

*As opposed to the contribution to the scattering fraction from double scattering, or from the (neglected) unpolarized term in the Compton scattering expression.

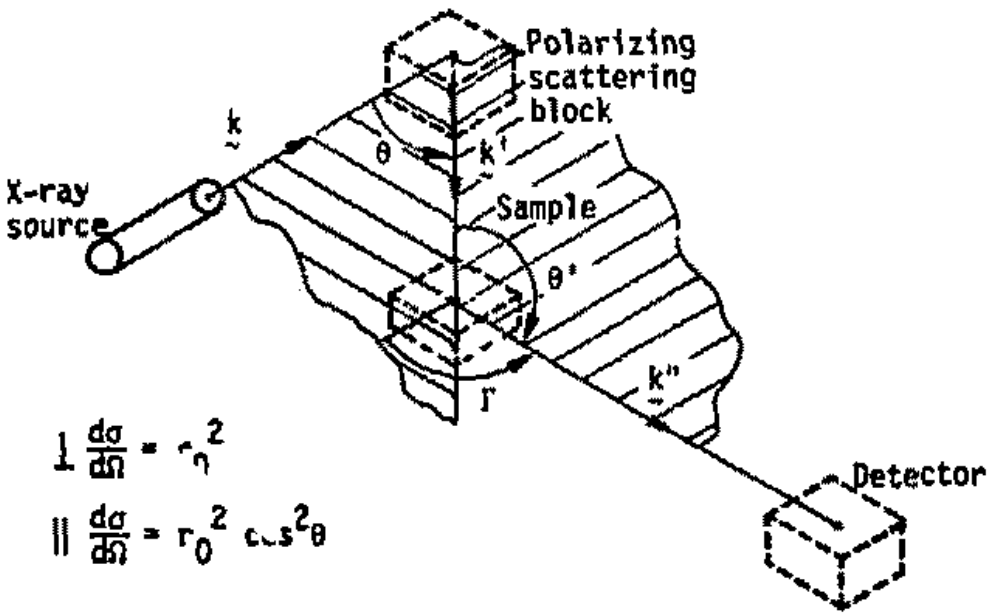

Fig. 1. Geometry resulting in minimum scatter from sample to detector. $\theta = \theta' = \Gamma = 90°$.

$$R_g = 2/3\ (\omega^2 + \omega'^2 + \gamma^2)$$

where ω, ω', and γ are respectively one-half the range of θ, θ', and Γ about 90°.

In any x-ray analysis the fluorescent x-ray intensity is proportional to the product of the amount of fluorescent species, the excitation flux intensity at the sample, the solid angle subtended by the x-ray detector, and an overall efficiency factor. These factors may be combined into the expression

$$I = C\ T_p\ d\Omega_p\ d\Omega_s\ d\Omega_d$$

where T_p is the polarizing scatterer thickness, $d\Omega_p$ is the solid angle subtended by the polarizing scatterer, $d\Omega_s$ is the solid angle subtended by the sample, $d\Omega_d$ is the solid angle subtended by the detector, and C is all other factors and efficiencies.

Although they are not identical, the solid angles above and the ω, ω', γ angular divergences are the result of the same physical constraints on geometry. (Similarly the intensities of both singly and doubly scattered radiation are functions of the thickness of the scatterer.)

An experimental demonstration of the functional relationship of these effects was obtained using a silver-target, transmission-anode x-ray tube (4) and an adjustable jig which kept x-ray source, polarizer, sample, and detector in the geometry shown in Fig. 1. Solid angle and angular divergence were varied by adjusting the distances between source, polarizer, sample, and detector while keeping the same size for each of these elements. The thickness and geometry of the polarizing scatterer could be varied by replacing one scatterer with another; in this case the interelement distances were varied in order to maintain solid angles and angular divergences at some value.

Figure 2 shows the measured scattering fraction and the relative fluorescent intensity, graphed as functions of the calculated scattering fraction due to geometry. The angular divergences were varied by changing the interelement distances. The data show that the fluorescent intensity is a strong function of changing geometry when compared to both the calculated geometric scattering fraction and the measured scattering fraction. In this data a large portion of the measured scattering is the result of double scattering in the polarizing scatterer and sample. A large loss in fluorescent intensity results from a small decrease in the scattering fraction.

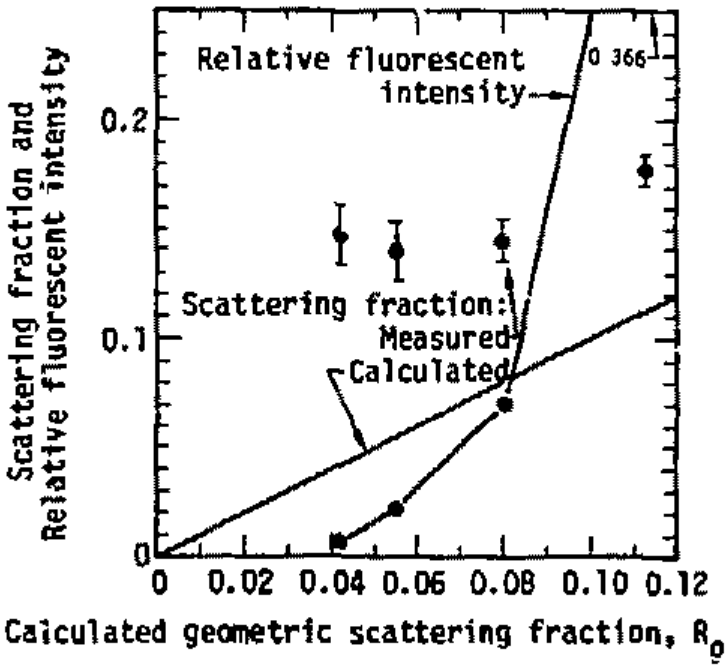

Fig. 2. Measured scattering fraction (defined in Table 1) and relative fluorescent intensity as functions of the calculated scattering fraction (R_g) for different experimental geometries. Data were taken with a 19 X 19-mm cylindrical polyethylene scattering block and a 6 X 6-mm cylindrical iron-tagged polyethylene sample. The fluorescent efficiency for the different geometries varies from 5×10^{-3} to 7×10^{-5}.

Multiple Scattering

X rays which scatter more than once either in the polarizing scatterer or in the sample are no longer as inhibited from scattering into the detector. A good expression for this effect is difficult to obtain in a general case. Calculations for special cases have been made. The ratio of second to first scattering at 90° for a sphere of radius R is (5)

$$R_s = \frac{44}{15} \pi \rho r_0^2 R \left[\frac{1 - e^{-\mu R}}{\mu R}\right]$$

where ρ is the electron density in the sphere and μ is the mass absorption coefficient. For polyethylene this becomes

$$R_s = 3 R \text{ (mm)}$$

when R is less than 10 mm. For this polarized geometry about three-fourths of the doubly scattered radiation that reaches the sample from the polarizer is polarized in the same plane as the singly scattered radiation. In addition, in the sample, doubly scattered radiation will tend to scatter away from the detector.

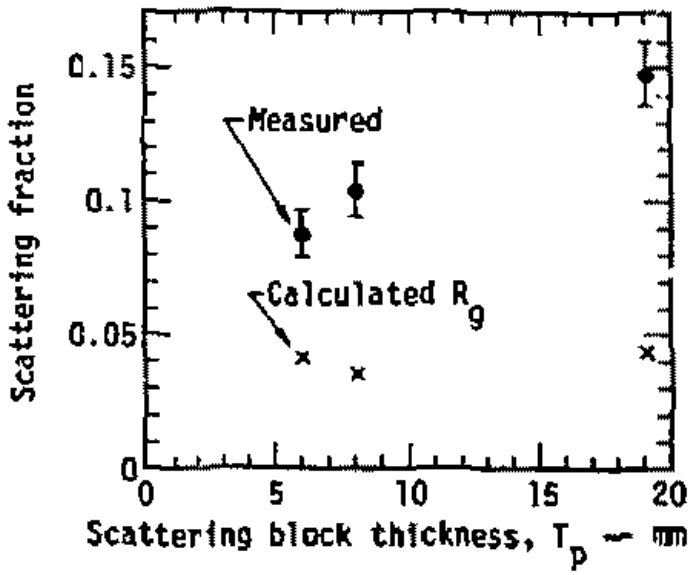

Fig. 3. Scattering fraction from various scatterers as a function of scatterer thickness T_p for the same geometric scattering fraction (R_g).

The results given here for a sphere can only be used as a rough indicator of the absolute amount of multiple scattering present in nonspherical shapes. However, the roughly linear dependence of such scattering on the thickness of the scatterer will usually still be obtained.

Figure 3 demonstrates the contribution to the scattering fraction of multiple scattering in the polarizer and sample, plotted as a function of polarizer thickness. All the polarizing scatterers used are polyethylene; all present an area to the x-ray source and sample equal to the thickness squared. Interelement distances were adjusted to keep the calculated geometric scattering fraction constant.

The nearly linear dependence of multiple scattering on scatterer thickness is evident. The contribution of multiple scattering in the polarizer to the scattering fraction sets a tight limit on the thickness of the polarizing scatterer. More importantly, multiple scattering in a thick sample limits the scatter rejection that can be obtained by polarized excitation.

Curved Polarizing Scatterer

These data and expressions indicate that in order to obtain a higher fluorescent efficiency at some fixed scattering fraction, the solid angles subtended by the elements must be increased without increasing the thickness of the scatterer or the angular divergences ω, ω', and γ. This can be done by using a curved polarizing scatterer.

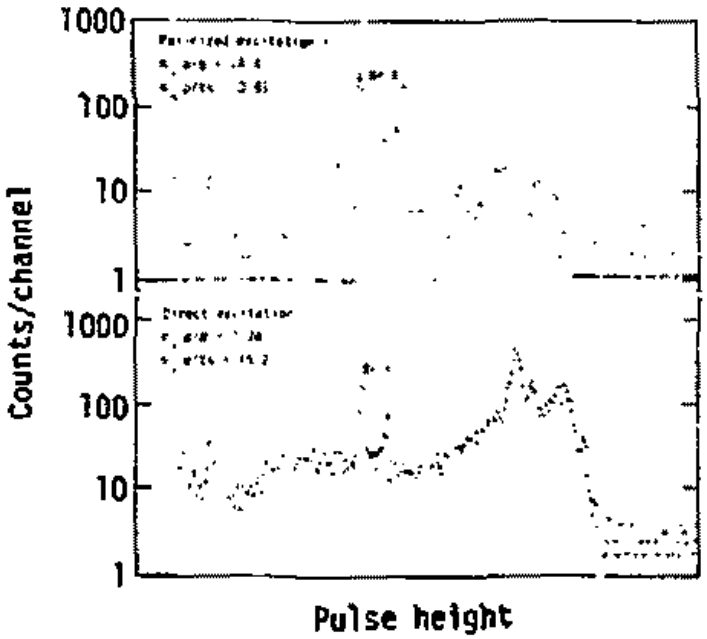

Fig. 4. Spectrum of bromine on several thicknesses of filter paper. A curved polarizer, 3 × 6 × 50 mm, was used. In the figure *p/b means peak-to-background; p/ts means* peak-to-total-scattering.

Consider a circle whose diameter is the line between x-ray source and sample, and consider a polarizing scatterer shaped to an arc of this circle. Every point along this scatterer will define a right triangle whose hypotenuse is the source-sample line. Angular divergence will be minimized since every source-scatterer-sample x-ray path traverses a right angle (the divergences are measured as deviations from 90°). Such a polarizer will have angular divergence comparable to a small block while presenting an increased solid angle to the x-ray source.

Such a polarizer was constructed from a 3 × 6 × 50-mm strip of polyethylene with a radius of curvature of 70 mm. This polarizing scatterer was compared with a 6-mm cube in a geometry for which the legs of the right triangle were 89 mm and 114 mm. The fluorescent efficiency was improved by a factor of 2.7 while the scattering fraction was unchanged. Figure 4 gives spectra of direct excitation and polarized excitation with this curved scatterer. The sample was bromine-impregnated filter paper, cut and folded to four layers in a 6 × 6-mm square and supported by cellophane tape. The scattering fraction calculated from this data is 0.063, or about 1.5 times the calculated geometric limit for this case. The fluorescent efficiency is about 2×10^{-4} in this configuration. The total scattered intensity is

reduced by a factor of 16 relative to the signal, while the reduction of background under the peak is only a factor of 10. This is partly due to the softening of the excitation flux spectrum, much of which is at a lower energy after scattering in the polarizer.

BORRMAN TRANSMISSION

The reduction of scattering in an x-ray fluorescence spectrum and the fluorescent efficiency are functions of several interrelated parameters for a scattering polarizer as shown above. Gains in background reduction are made at high cost in overall efficiency. Because of this a second polarizing effect, anomalous Borrman transmission, has been investigated.

Borrman transmission is an energy-selective, polarization-selective effect observed in single crystals of high quality. The transmission effect is obtained when the nodes of the x-ray wave pattern coincide with the crystal lattice sites so that photoelectric absorption at these sites is minimized. Moreover, theory predicts that the absorption is considerably greater for x rays linearly polarized in the plane defined by the transmitted and diffracted beam than for x rays polarized normal to that plane. This effect thus fixes the plane of polarization with respect to the crystal planes. The energy of x rays that are transmitted depends on the spacing of lattice sites in the beam's direction of travel. The wavelength of the transmitted beam depends on the angle of the crystal with respect to the beam. (This wavelength is described by the same expressions that are used for Laue diffraction.)

Other experimenters have constructed such a polarized x-ray source for copper K_α x rays from the target of an x-ray tube. (6) The crystal used was pure germanium; the measured polarization from this system was greater than 99 percent. Although this polarized source was built to study crystal quality, it could be used without modification as a low-energy excitation source for x-ray fluorescence analysis.

For general x-ray fluorescence problems, however, higher-energy Borrman transmission must be demonstrated. Transmission in a germanium crystal, 0.93-mm thick and cut along the (111) planes, has been reported to be 1.2×10^{-4} of the incident flux at 21.5 keV. (7) This is in the same range as the efficiency for scattering polarimeters discussed earlier. The polarization of the transmitted x rays was not measured in that experiment.

To measure the polarization this same germanium crystal was mounted in the rotating goniometer seen in Fig. 5. The x-ray source is a silver-target, transmission-anode tube run at 40 kV. The goniometer allowed the adjustment of the beam-crystal

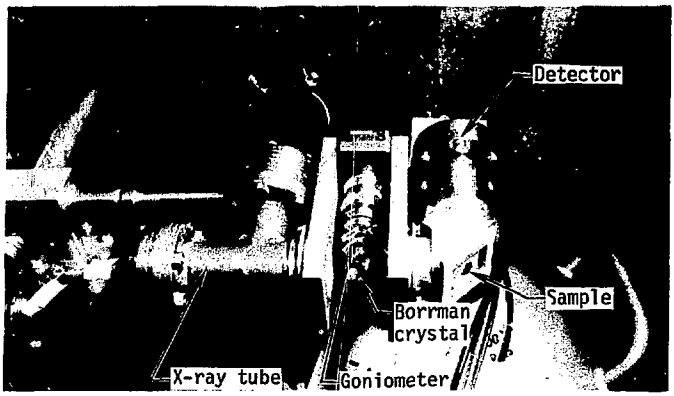

Fig. 5. X-ray tube, germanium crystal, sample, and detector used in the Borrman transmission experiments, shown in a rotating goniometer in the geometry for minimum scatter from sample to detector. Transmission energy is varied by rotating the crystal with respect to the beam. The polarization at the sample is changed by rotating it about the beam direction.

angle to obtain transmission of the silver characteristic K x rays. Collimation was provided by 3-mm-diam holes in 10-mm-thick tungsten collimators, 25 mm on each side of the crystal and in front of the detector. Polarization was measured by placing 3-mm-thick Lucite plastic at the sample position; rotating the crystal, goniometer, and holder with respect to the detector; and measuring the scattered flux at the detector.

The results of transmission measurements are shown in Fig. 6. Plotted there is the intensity as a function of angle in three energy intervals of equal width: one centered at the silver K_α energy, one centered at the silver $K\beta$ energy, and one at the electron end-point energy (40 keV). Figure 7 compares the transmission spectrum at 42° to the spectrum of the incident beam.

Due to the relatively open collimation of the transmitted beam, both the silver K_α and $K\beta$ x rays are transmitted for some crystal angles. Restricting the collimation would narrow the energy distribution of the transmitted beam. The ratio of strength of the Borrman-transmitted x rays to the strength of the filtered x rays is a strong function of the total attenuation in the crystal. The differential attenuation of the two polarization states in the transmitted beam also depends on the total attenuation.

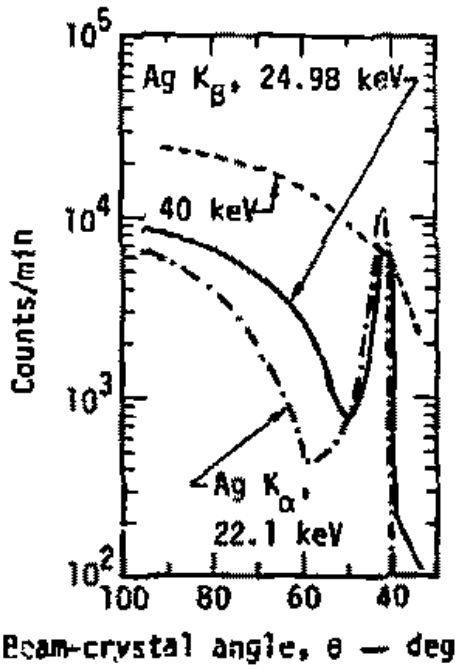

Fig. 6. X-ray intensity of filtered, Borrman-transmitted beam as a function of the angle between beam and crystal in three energy intervals.

Figure 6 shows that the Borrman transmission at 25 keV is only a factor of 30 higher than the intensity of the normally filtered beam. Also, the strength of the filtered, hardened beam at 40 keV is high. These data indicate that although the crystal did Borrman-transmit, it is not thick enough to act as a strong filter at these higher energies.

The polarization measured had a minimum scatter into the detector when the detector-sample axis and the axis of rotation of the crystal were parallel. The ratio of intensity perpendicular to parallel in the scatter peaks was 3.4 ± 0.3. This is considerably less than the value of ~200 measured at lower energies (copper K_α) where the normal attenuation in the crystal is much greater. (6) Thicker crystals or crystalline material of higher atomic number will be necessary to provide a filtered, polarized beam from an x-ray tube run at high voltage or with high-Z targets.

For comparison with the transmission spectrum, Fig. 7 includes the pulse-height spectrum of scattering from a scattering polarizer. Borrman transmission sharpens and filters the beam, while scattering shifts some x-ray energy downward and generally tends to soften the excitation flux. This suggests that for equal polarization quality Borrman-transmission excitation will result in a higher peak-to-background ratio than that from a scattering polarizer. Table 2 summarizes and compares characteristics of the two polarization methods.

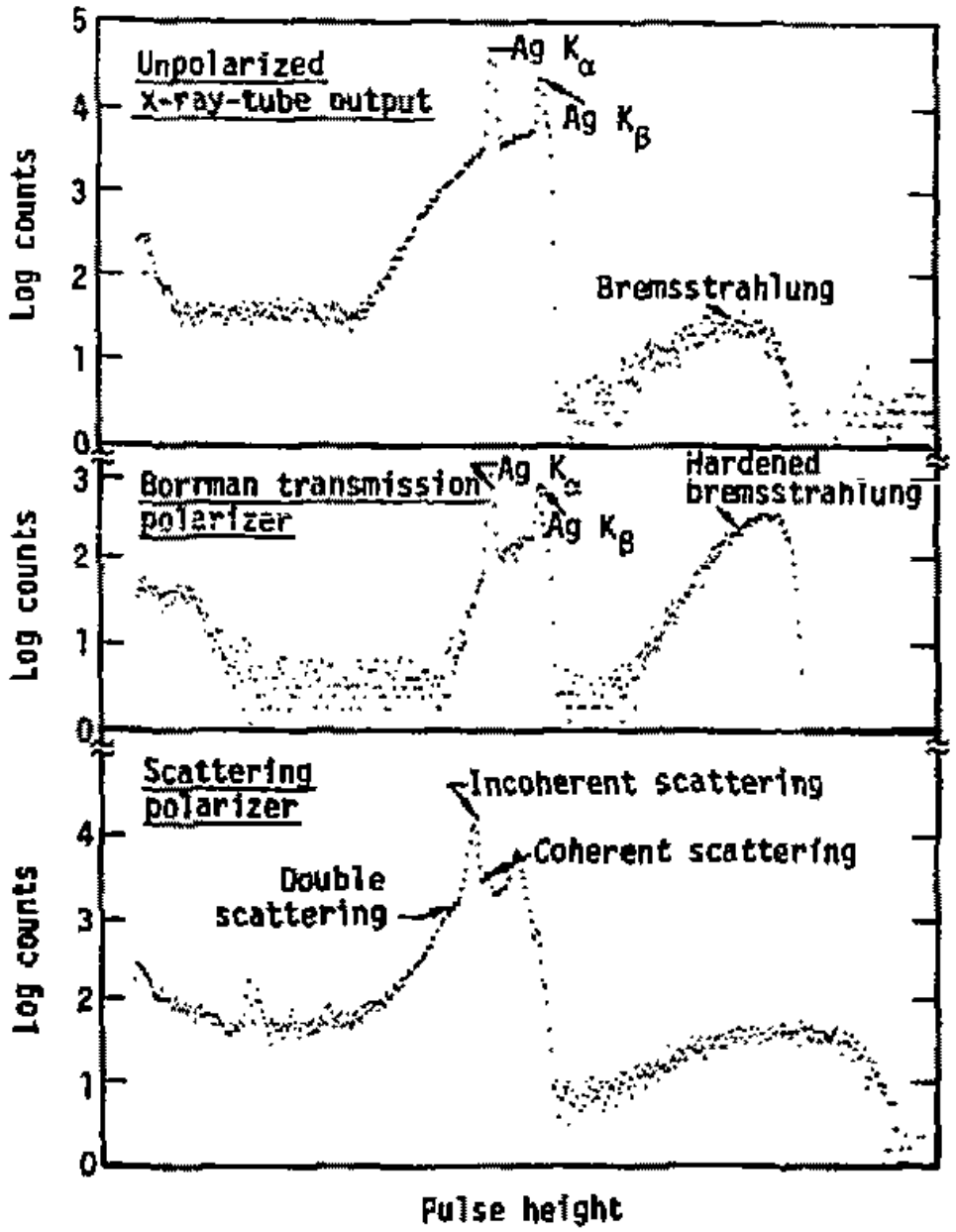

Fig. 7. Pulse-height spectra of (top) the output of the silver-target, transmission-anode x-ray tube; (middle) that output filtered with a Borrman-transmitting crystal (1-mm Ge); (bottom) that output scattered from a large scattering polarizer (19-mm-diam, 19-mm-long polyethylene cylinder).

Table 2. Comparison of scattering and Borrman polarizers.

Feature	Scattering polarization	Borrman transmission
Polarization vs efficiency	Polarization efficiency is limited by double scattering and beam divergence. However, a high efficiency and low polarization are possible.	Efficiency is limited by crystal quality. Polarization is controlled by crystal thickness.
Energy characteristics of polarized beam	Energy of scattered x rays is less than in the unpolarized beam. The spectrum is softened.	Energy of transmitted x rays is unchanged and spectrum is highly filtered.
Source-Polarizer-Sample divergence	Divergence of both the source and polarized beam must be limited by collimation in both dimensions for high polarization.	Divergence of polarized beam is limited by the crystal in one dimension. Must be collimated in other dimension.
Sample size	Sample size limits scattering rejection by double scattering into detector	Same as scattering polarization.
Sample-detector divergence	Must be limited by collimation.	Same as scattering polarization

REFERENCES

1. J.C. Young, 1973 Pacific Conf. on Chemistry and Spectroscopy, San Diego, CA, Nov. 1973.

2. T.G. Dzubay, B.V. Jarrett, and J.M. Jaklevic, "Background Reduction in X-Ray Fluorescence Using Polarization," Nucl. Instr. and Meth. 115, 297 (1974).

3. R.H. Howell, J.L. Cate, and W.L. Pickles, X-Ray Polarization Studies, Lawrence Livermore Laboratory, Rept. UCRL-50007-73-2 (1974).

4. W.L. Pickles and J.L. Cate, Jr., "Quantitative Nondispersive X-Ray Fluorescence Analysis of Highly Radioactive Samples for Uranium and Plutonium Concentration," Advances in X-Ray Analysis 17, 337 (1973).

5. P. Kirkpatrick, "Double Scattering of Polarized X-Rays," Phys. Rev. 52, 1201 (1937).

6. H. Cole, F.W. Chambers, and C.G. Wood,"X-Ray Polarizer," J. Appl. Phys. 32, 1942 (1961).

7. W.L. Pickles and J.H. Elliott, Fiscal Year 1973 Summary Report for the USAEC Division of Applied Technology — Environmental Analysis, Lawrence Livermore Laboratory, Rept. UCRL-51422 (1973).

DISTRIBUTION

LLL Internal Distribution

Roger E. Batzel	
J. Anderson	
N. A. Bonner	
T. A. Boster	
D. C. Camp	
G. W. Campbell	
J. L. Cate	5
T. M. Distler	
D. W. Dorn	
J. H. Elliott	
J. R. Gaskill	
R. Gunnink	2
R. W. Hoff	
R. H. Howell	5
M. Knezevich	
G. Mackanic	
M. M. May	
J. A. Miskel	2
W. E. Nervik	
J. B. Niday	
J. L. Olsen	
H. W. Patterson	
W. L. Pickles	10
C. T. Prevo	
I. D. Procter	
R. C. Ragini	
R. W. Ryon	
D. C. Sewell	
R. C. Schroeder	
D. R. Slaughter	
R. D. Taylor	
J. F. Tinney	2
C. E. Violet	
J. C. Walden	
TID File	30

External Distribution

R. R. A. Atneosen
Western Washington State College
Bellingham, Washington

W. C. Bartels, Chief, Technology Branch, Div. of NUMS — 10
U.S. Atomic Energy Commission
Washington, D.C.

H. Blosser
Michigan State University
East Lansing, Michigan

External Distribution (Continued)

R. Bragg
University of California
Berkeley, California

C. G. Clayton
Atomic Energy Research Establishment
Berkshire, United Kingdom

A. E. Evans
Los Alamos Scientific Laboratory
Los Alamos, New Mexico

R. W. Foster
E.I. DuPont de Nemours and Co.
Aiken, South Carolina

E. E. Fowler
U.S. Atomic Energy Commission
Washington, D.C.

A. Galonsky
Michigan State University
East Lansing, Michigan

A. Gibbs
E.I. DuPont de Nemours and Co.
Aiken, South Carolina

F. S. Goulding
University of California
Lawrence Berkeley Laboratory
Berkeley, California

J. Glancy
U.S. Atomic Energy Commission
Washington, D.C.

A. Higinbotham
Brookhaven National Laboratory
Upton, Long Island, New York

R. Hinds
Yankee Atomic Electric
Westboro, Massachusetts

J. W. Jaklevic
University of California
Lawrence Berkeley Laboratory
Berkeley, California

R. Jarozeski
Nuclear Fuel Services, Inc.
West Valley, New York

External Distribution (Continued)

E. Kashy
Michigan State University
East Lansing, Michigan

R. G. Keepin
Los Alamos Scientific Laboratory
Los Alamos, New Mexico

R. P. Larsen
Argonne National Laboratory
Argonne, Illinois

S. Lawroski
Argonne National Laboratory
Argonne, Illinois

D. E. Leyden
The University of Georgia
Athens, Georgia

A. Medcalf
Pacific Gas and Electric Company
San Francisco, California

S. G. Medcalf
Atlantic Richfield Hanford Company
Richland, Washington

J. Menzel
International Atomic Energy Agency
Vienna, Austria

D. J. Nagel
Naval Research Laboratory
Washington, D.C.

T. D. Reilly
Los Alamos Scientific Laboratory
Los Alamos, New Mexico

C. T. Sanders
Oak Ridge National Laboratory
Oak Ridge, Tennessee

R. B. Sewell
Consumers Power Company
Jackson, Michigan

T. Shea
U.S. Atomic Energy Commission
Washington, D.C.

A. J. Skinner
U.S. Atomic Energy Commission
Aiken, South Carolina

External Distribution (Continued)

R. T. Smokowski
Nuclear Fuel Services, Inc.
West Valley, New York

D. Snape
Philips Electronics Industries Ltd.
Toronto, Ontario

D. L. Taylor
California State University, Humboldt
Arcadia, California

J. Umbarger
Los Alamos Scientific Laboratory
Los Alamos, New Mexico

A. H. E. Von Baeckmann
Gesellschaft Fuer Kernforschung MBH
Karlsruhe, Germany

G. R. Waterbury
Los Alamos Scientific Laboratory
Los Alamos, New Mexico

W. Willoughby II
South Carolina Electric and Gas
Columbia, South Carolina

Technical Information Center 2
Oak Ridge, Tennessee

KAD/lc